




RESEARCH ARTICLE

In vivo grading of lipids in fatty liver by near-infrared autofluorescence and reflectance

José Lifante^{1,2}  | María de la Fuente-Fernández¹ | Marta Román-Carmena² |
 Nuria Fernandez¹ | Daniel Jaque García^{1,2}  | Miriam Granado¹ |
 Erving Ximendes^{1,2} 

¹Nanomaterials for Bioimaging Group (nanoBIG), Universidad Autónoma de Madrid, Madrid, Spain

²IRYCIS, Madrid, Spain

Correspondence

Erving Ximendes, Nanomaterials for Bioimaging Group (nanoBIG)
 Departamento de Física de Materiales
 C-04 Facultad de Ciencias, Universidad Autónoma de Madrid Avenida Francisco Tomás y Valiente 7 28049 Madrid, Spain.
 Email: erving.ximendes@uam.es

Funding information

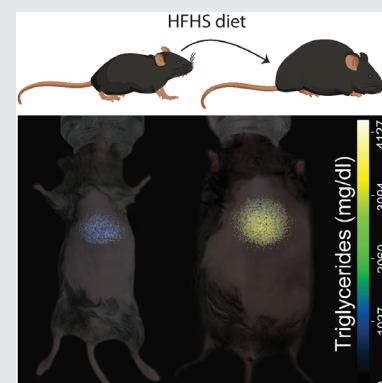
Ministerio de Ciencia e Innovación,
 Grant/Award Number: IJC2020-045229-I;
 Ministerio de Ciencia e Innovación,
 Grant/Award Number:
 NANONERVPID2019-106211RB-I00

Abstract

The prevalence of nonalcoholic fatty liver (NAFLD) is rapidly increasing worldwide. When untreated, it may lead to complications such as liver cirrhosis or hepatocarcinoma. The diagnosis of NAFLD is usually obtained by ultrasonography, a technique that can underestimate its prevalence. For this reason, physicians aspire for an accurate, cost-effective, and noninvasive method to determine both the presence and the specific stage of the NAFLD. In this paper, we report an integrated approach for the quantitative estimation of the density of triglycerides in the liver based on the use of autofluorescence and reflectance signals generated by the abdomen of obese C57BL6/J mice. Singular value decomposition is applied to the generated spectra and its corresponding regression model provided a determination coefficient of 0.99 and a root mean square error of 240 mg/dl. This, in turn, enabled the quantitative imaging of triglycerides density in the livers of mice under in vivo conditions.

KEYWORDS

autofluorescence, nonalcoholic fatty liver, reflectance, singular value decomposition, spectra



1 | INTRODUCTION

In vivo fluorescence imaging (FI) has become a well-grounded tool in preclinical research and has made possible the development of new procedures for early diagnosis, control over therapies and, even, improvement of efficacy of surgical procedures [1–5]. In most

cases, FI is based on the use of light-excited exogenous fluorophores, such as organic dyes and luminescent nanoparticles. And for this reason, the scientific community has been very active in the design and synthesis of many biocompatible luminescent probes [6, 7]. Additionally, to avoid problems such as limited penetration depth or undesired background signal caused by

This is an open access article under the terms of the [Creative Commons Attribution](https://creativecommons.org/licenses/by/4.0/) License, which permits use, distribution and reproduction in any medium, provided the original work is properly cited.

© 2022 The Authors. *Journal of Biophotonics* published by Wiley-VCH GmbH.

tissue autofluorescence (TAF) and tissue reflectance, FI imaging started to move its operational spectral range from the visible to the infrared region. Indeed, many of the recently published works of literature report on the potential of FI at the preclinical level using imaging systems that operate within the so-called biological windows (BW), that is, infrared spectral regions where tissues become partially transparent.

Despite its relatively low signal when compared to the whole electromagnetic spectrum, TAF in the BWs is not completely negligible. While many consider TAF as one of the main drawbacks of infrared FI, as it impacts negatively on both contrast and resolution, its negative perception is often related to the type of application that one intends to accomplish [8]. Indeed, TAF can result especially appropriate to provide information on tissue properties and metabolic activity and, hence, it can work as a tool for remote and contactless tissue diagnosis [9, 10]. Most of the demonstrations of the diagnostic potential of TAF, however, are in the visible spectral domain, where a vast library of fluorophores and TAF bands does exist (see Figure 1). The picture is completely changed when it comes to the infrared. Due to the relatively low intensity, there are fewer systems suitable for its detection and, therefore, a reduced number of studies on infrared TAF. In addition, few fluorophores (such as neuromelanin, see Figure 1) have their autofluorescence signal peaking in the II-BW [11]. Such a gap in knowledge is inopportune as recent experiments have demonstrated that

there is a long infrared tail of TAF that leads to non-negligible contributions in both the first BW (I-BW, 750–900 nm) and second BW (II-BW, 1000–1400 nm).

Very recently, some works have come into scene demonstrating the strong correlation between the tissue's optical properties and its lipid content. Among those properties, tissue reflectance and absorption stand out as one of the most investigated. Their correlation with lipid content opens new avenues toward noninvasive detection and monitoring of diseases associated with the superabundance of fat such as hepatic steatosis, also known as nonalcoholic fatty liver disease (NAFLD). Within NAFLD we have to distinguish between alcoholic fatty liver disease (AFLD), a condition that affects more than 90% of heavy drinkers, and NAFLD, the most prevalent chronic liver disease in Western countries, especially among obese individuals, that affects 20%–30% of the population worldwide [29–32]. Although the pathogenesis of NAFLD is not completely understood, it is known that it starts with the accumulation of triglycerides within the hepatocytes producing simple steatosis. This simple steatosis may progress to various degrees of necrotic inflammation producing nonalcoholic steatohepatitis (NASH), a condition characterized by inflammation, cellular death, and fibrosis [33].

Depending on lipid accumulation, NAFLD can be graded into different stages, with steatosis lower than 5% being considered normal and steatosis higher than 5% being considered Grade 1 [34]. The absence or scarcity of early symptoms makes that most individuals affected by

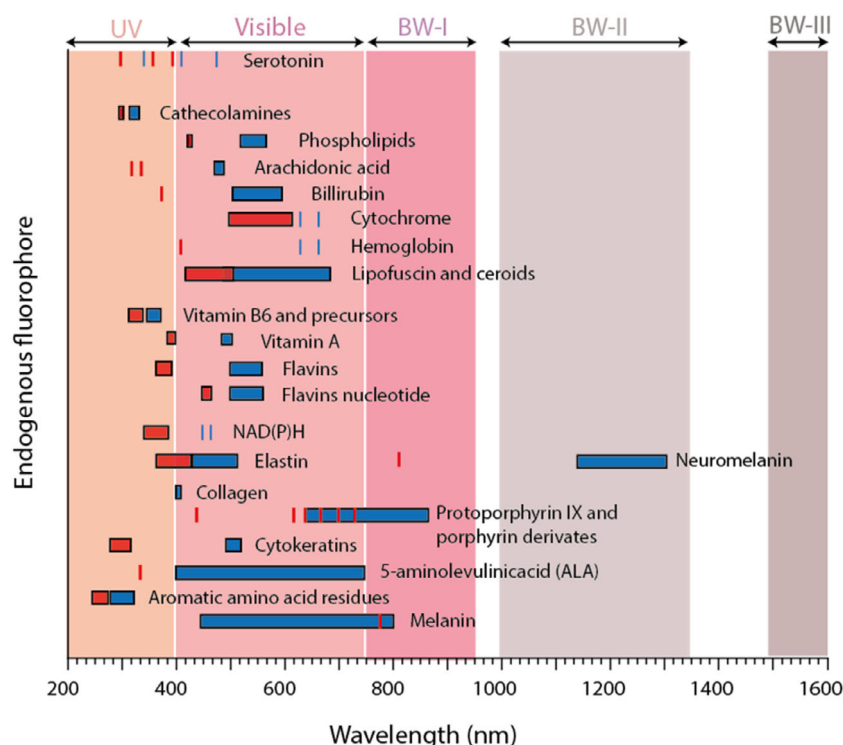


FIGURE 1 Fluorophores present in tissues with known excitation (dashed areas) and emission (solid areas) autofluorescence bands. The spectral extension of visible and biological windows is indicated. Data taken from the references [11–28]

NAFLD are incidentally diagnosed due to tests of liver function or to hepatomegaly noted in unrelated medical conditions. This fact increases the chances that the disease will progress to NASH producing, in some cases, severe complications such as cirrhosis, liver cancer, and esophageal varices. Apart from the scarcity of symptoms, another handicap for NAFLD diagnosis is the lack of reliable biomarkers to detect or predict liver inflammation, which makes necessary the use of additional diagnosis methods such as liver biopsy, which remains the current gold standard since it allows to quantify both the lipid content and inflammation, thus permitting an adequate prognostic classification of the disease. However, this method has several drawbacks which include its invasiveness, high cost, and sample variability [35]. Thus, the most challenging endpoint is to find an accurate noninvasive method to determine the stage of NAFLD and thus be able to offer a more accurate prognosis and therapeutic options to each patient. In this regard, different imaging techniques such as computed tomography, ultrasonography, and magnetic resonance imaging already exist and might play a role in the detection or progress evaluation of NAFLD [36]. Among them, abdominal ultrasound is the most widely available, but its diagnostic sensitivity is lower when there are mild degrees of hepatic fatty infiltration. Indeed, the lower limit for the reliable detection of steatosis through ultrasound is 30%, which means that those cases that are in the early stages of the disease cannot be diagnosed by this technique [37]. Likewise, computed tomography is also reported to have a specificity of 100% when the fat content is greater than 30%. In addition, the use of ionizing radiation brings with it additional complications. Magnetic resonance imaging with spectroscopy, in turn, is the preferred method for the detection and quantification of liver fat content but its high cost makes it difficult to be systematically used in all patients suspected of suffering from this disease [38]. Thus, by the present day, presenting a cost-effective technique, such as II-BW imaging, capable of detecting NAFLD at an early stage is highly beneficial for healthcare. Although TAF and reflectance studies have certainly given important insights to the study of liver function in physiological conditions [30, 39, 40], when retrieving the literature, little is found on their concomitant use for the assessment of the development of NAFLD. And the few works that attempt to do it are advancing the subject at the *ex vivo* level [41]. The lack of *in vivo* studies of NAFLD by infrared imaging can be mostly attributed to the absence of a proper experimental approach that allows for quantitative analysis of *in vivo* images obtained in the absence of any contrast agents. Unsurprisingly, such quantitative analysis is not an easy task as it requires accurate evaluation of the relative contributions of TAF and reflectance and the design and development of new optical systems.

The not-so-extensive use of II-BW imaging for tissue diagnosis can be partially attributed to the lack of spectral resolution in most cost-effective infrared imaging systems. However, in recent years, Hyperspectral Imaging (HSI) has come into scene as a solution for such a limitation. HSI is an automated spectrally sensitive technology that integrates imaging and conventional spectroscopy in such a way that it provides complementary information from both domains [42–45]. It makes possible the spectral analysis of II-BW endogenous signal with a sub-micrometer spatial resolution [30, 31]. This imaging capability, in combination with the penetration ability of II-BW radiation into tissues, makes possible the spectral analysis of the optical properties of internal organs, such as the liver. Thus, in this work, we evaluate the potential of infrared imaging for *in vivo* diagnosis of NAFLD. Hyperspectral infrared *in vivo* imaging together with dual-wavelength excitation has made possible accurate determination of the relative contribution of tissue reflectance and autofluorescence to the non-specific endogenous signal in *in vivo* images. We then applied our approach to monitoring the development of NAFLD in a murine model. The time-course of II-BW reflectance and autofluorescence is correlated with the presence of triglycerides in both liver and surrounding tissues. Advanced data analysis based on dimensionality reduction is then applied for a fast determination of the density of triglycerides in the liver.

2 | METHODS

2.1 | Illumination

An 808 nm fiber-coupled laser diode was utilized to illuminate a 16 weeks old control C57BL6/J male mouse while a short-pass filter (cut-off wavelength of 850 nm) is used to block the long-wavelength tail of the laser source. Additionally, a Nd³⁺ sample is introduced in between the exit of the laser fiber and the surface of the animal. Under such conditions, neodymium ions are then excited and produce a significant emission at 1045 nm. Hence, dual-wavelength excitation is achieved. The introduction of neodymium is justified by the well-reported maximization of reflection of II-BW light by tissues with high content of lipids at precisely 1045 nm [46]. In these circumstances, the tissue is then expected to reflect the radiation at 1045 nm while simultaneously generate autofluorescence.

2.2 | Optics and hyperspectral imaging

To avoid the perturbation caused by the laser (808 nm) light reflected by tissues in the overall signal, a long-pass

filter (Thorlabs FL0850) was put before the detection system. Both the 808 nm excited TAF and the 1045 nm reflected signal were then acquired by a shortwave infrared camera (ZephIR™ 1.7). For building the II-BW autofluorescence hyperspectral image a set of lenses was used to image the pupil on a Bragg tunable filter that tuned the imaging wavelength, λ , from 900 up to 1400 nm. This filtered light was then focused, by a second lens, on the infrared camera to produce a monochromatic image. Under these circumstances, a 3D spatial map of spectral variation, that is, a HSI cube, was obtained: the first two dimensions of the cube providing spatial information and the third accounting for the spectral information [47, 48]. The intensity values of a particular pixel in a HSI cube characterized its spectral fingerprint. Thus, by a careful selection of the region of interest, one could plot the corresponding luminescence spectrum.

2.3 | Discrimination of contributions from tissue layers in HSI

The *in vivo* II-BW image of a mouse was acquired while the layers of tissues above the liver (mouse in supine position) were sequentially removed (Figure 2D). Once the *in vivo* II-BW spectrum of the exposed liver

(in absence of skin and muscle above it) was obtained, the animal was sacrificed and a last straightforward acquisition of the II-BW spectrum of the liver was performed under *ex vivo* conditions to eliminate possible contributions of tissues found underneath the liver in normal conditions.

2.4 | Study of effects of high-fat-high-sugar diet

To explore the potential of HSI in the detection of NAFLD at different stages of development, 36 C57BL6/J male mice of same age (16 weeks old) were equally separated into two main groups: the mice that were subjected to a high-fat-high-sugar diet (HFHS), and the mice that were subjected to a standard diet (hereafter, healthy). Each of these main groups, in turn, was divided into six subgroups according to the time points in which they were sacrificed (Figure 3A). Such time points were computed relative to the moment in which the HFHS diet started in the first main group. They were namely: 1, 3, 6, 12, 26, and 52 weeks. Thus, for each stage of development of NAFLD, we acquire the II-BW endogenous spectra of three healthy and three HFHS mice. These spectra, in turn, were divided by their intensity integrated in the 900–1400 nm range for normalization.

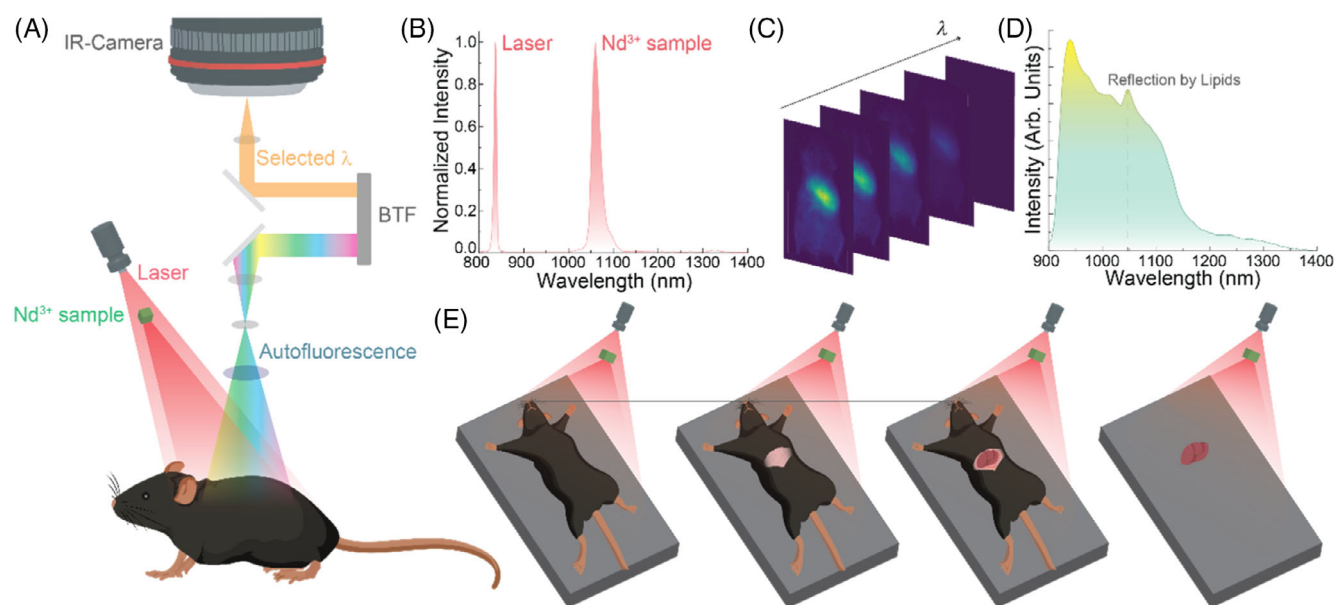


FIGURE 2 Hyperspectral imaging (HSI) of the liver of a C57BL6/J mouse. (A) Schematic representation of the HSI system used in this work. (B) Emission spectra of the two irradiating sources of light. While the laser is expected to cause the generation of NIR autofluorescence, the Nd³⁺ emission is expected to be reflected by the animal tissues. (C) Representative stack of narrowband fluorescence images of 16 weeks old control C57BL6/J male mouse. (D) Spectrum corresponding to the liver as obtained by averaging the pixel intensities of the region of interest of each mouse. A signal-to-noise ratio of approximately 15 was observed in all measurements. (E) Schematic representation of the steps followed to determine which layers of tissue are responsible for the reflectance peak characteristic of the lipids

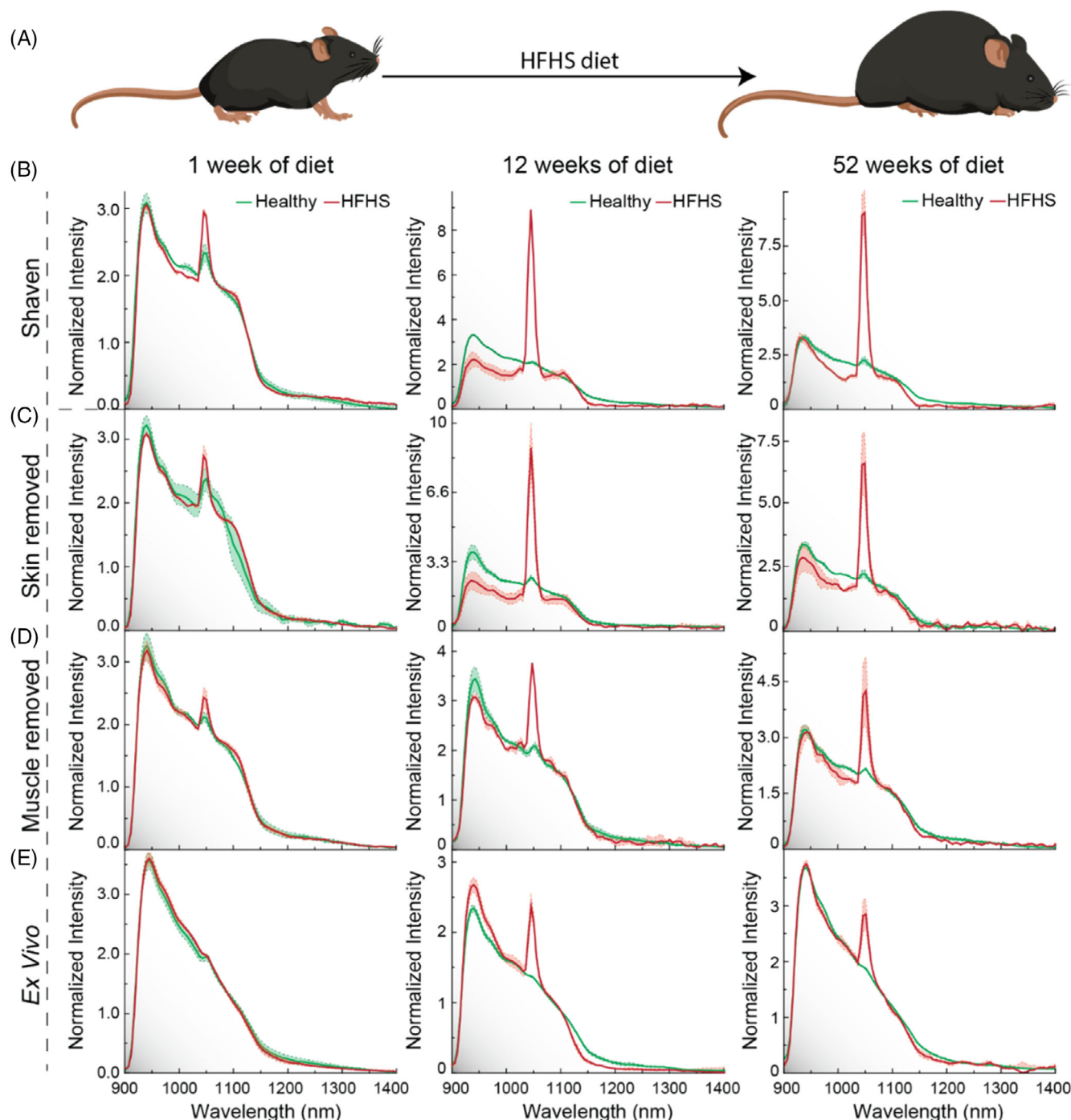


FIGURE 3 Influence of nonalcoholic fatty liver on the II-BW endogenous spectrum. (A) Schematic representation of the fattening of mice undergoing the high-fat-high-sucrose (HFHS) diet. Average II-BW spectra obtained at three time points of the HFHS diet (1 week, 12 weeks, and 52 weeks) with three replicates of mice that: (B) were only shaved; (C) had their skin removed while still leaving subcutaneous fat; (D) had their skin and muscle removed; and (E) had been sacrificed and their livers were exposed under ex vivo conditions. The ex vivo measurements were performed immediately after sacrifice, taking approximately 40 min to be completed. The semi-transparent green and red regions correspond to the standard deviation of the spectra in each of the groups

2.5 | Singular value decomposition

Singular value decomposition (SVD) is a technique capable of reducing the dimensionality of a dataset through

the factorization of the dataset matrix [49]. It identifies and orders the dimensions along which data points exhibit the most variation [50]. It is suitable for regression and classification problems where the number of

measurements is relatively low. Thus, after removing the wavelengths in which no significant emission was observed (i.e., beyond 1200 nm), SVD was applied to the dataset and the results are included in Figure 4A–D.

2.6 | Determination of biomedical parameters

The day before obtaining the II-BW spectra, mice were subjected to overnight fasting. Afterwards, glycemia was determined by tail puncture using the glucometer Glucocard G+ Meter (Arkray Factory, Inc). After sacrifice, blood was collected in tubes containing 1.5 mg/ml EDTA. Plasma was obtained after centrifugation at 4°C and 2000 g 3000 rpm for 20 min and used to determine the circulating levels of total lipids (hereafter L_{plasma}), cholesterol (CL_{plasma}), triglycerides (TG_{plasma}) by colorimetric assays following the manufacturer's instructions (Spin React S.A.U).

2.7 | Quantification colorimetric assay

The triglycerides contents in the livers of all the animals that were studied were obtained by performing a quantification

colorimetric assay. Briefly, a total of 100 mg of liver were homogenized in 300 μ l of phosphate-buffer saline (PBS) and centrifuged at 4°C during 10 min. The supernatant was diluted five times and used to measure triglycerides with a commercial kit (1001313, Spin React S.A.U) after following the manufacturer's instructions. Moreover, to determine the accumulation of lipids in the liver, a staining with Sudan III was performed. Liver samples were fixed with 4% paraformaldehyde in PBS for 24 h, washed with PBS + 30% sucrose for at least 8 h and included into optimal cutting temperature (OCT) resin. These samples were cut into 3 μ m sections and incubated for 24 h with Sudan III. Nuclei were counterstained with hematoxylin for 1 min. Images were acquired using a Leica light microscope fitted with 40 \times 0.65 NA objective.

2.8 | In vivo grading of lipids

To give a reasonable demonstration of this concept, we first expressed right singular vector (RSV_1) on the original basis of measurements (i.e., of intensities at different wavelengths $I_j[\lambda]$) to know exactly how to combine the fluorescence images and apply the linear function that described the regression model. To do so, a mask layer

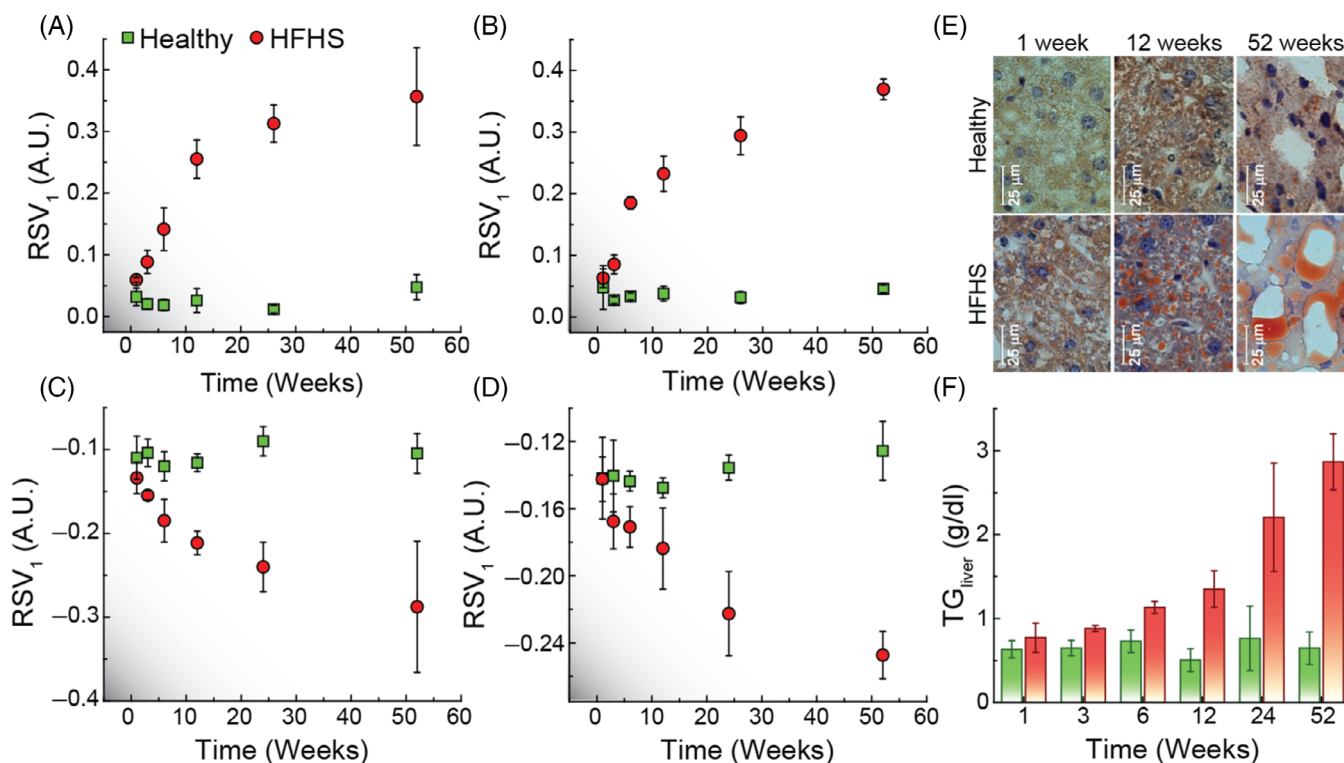


FIGURE 4 Ratiometric analysis of the autofluorescence spectra. Time dependence of the RSV_1 as obtained in (A) shaven, (B) “skin removed,” (C) “muscle removed,” and (D) “ex vivo” conditions. The number of replicates in each of the graphs was set to be equal to 3. (E) Histological images acquired with the livers of mice sacrificed at different time points of the HFHS diet. (F) Average density of triglycerides in the livers of the two groups of mice at different time points of their diets. The error bars correspond to the standard deviation

was applied to all their narrowband near-infrared images so that only the signal of the liver could be seen at different wavelengths. Then, each pixel of these narrowband images was normalized to the average intensity of its corresponding spectrum and was summed according to Figure 5C. After applying the linear regression model to the resulting image, the outcome of such an operation was then an image that reflected the triglycerides density in the liver. When superimposing it to the optical photos taken of the mice in the experiment and applying a pseudocolor scale, the result is what is depicted in Figure 5E. The subsequent analysis was then all based on the nonnegative pixels (i.e., the ones that survived the mask layer).

2.9 | Animal experimentation

Procedures involving animal experiments were approved by the regional authority for animal experimentation of the Comunidad de Madrid and were conducted in agreement with the Universidad Autónoma de Madrid Ethics Committee, in compliance with the European Union directives 63/2010UE and Spanish regulation RD 53/2013.

3 | RESULTS AND DISCUSSION

To elucidate the intrinsic in vivo II-BW endogenous signal (hereafter always referring to the signal obtained in the absence of contrast agents) of the liver, the experimental procedure depicted in Figure 2A, where a beam constituted by a 808 nm and a 1045 nm laser lines was set to illuminate the small animal (Figure 2B), was followed. Figure 2C shows a set of monochromatic infrared images corresponding to a 16 weeks old control C57BL6/J male mouse where its liver is evidenced with a strong II-BW autofluorescence [11]. The analysis of the hyperspectral cube at the liver's position provides its spectrum and is depicted in Figure 2D. It consists of a long tail extending from 900 to 1400 nm (corresponding to TAF) and a narrow peak generated by the reflection of the 1045 nm excitation line [8, 11]. In principle, the relative contribution of the 1045 nm peak could serve as an indicator of the relative content of lipids in tissues and, therefore, of the presence of NAFLD. However, due to the presence of layers of skin and muscle between the liver and the detection system, the value of such parameter is not limited to the content of lipids in the liver only but also the lipids in all the intermediate tissues. To address this source of error, we designed the experiment schematically represented in Figure 2D.

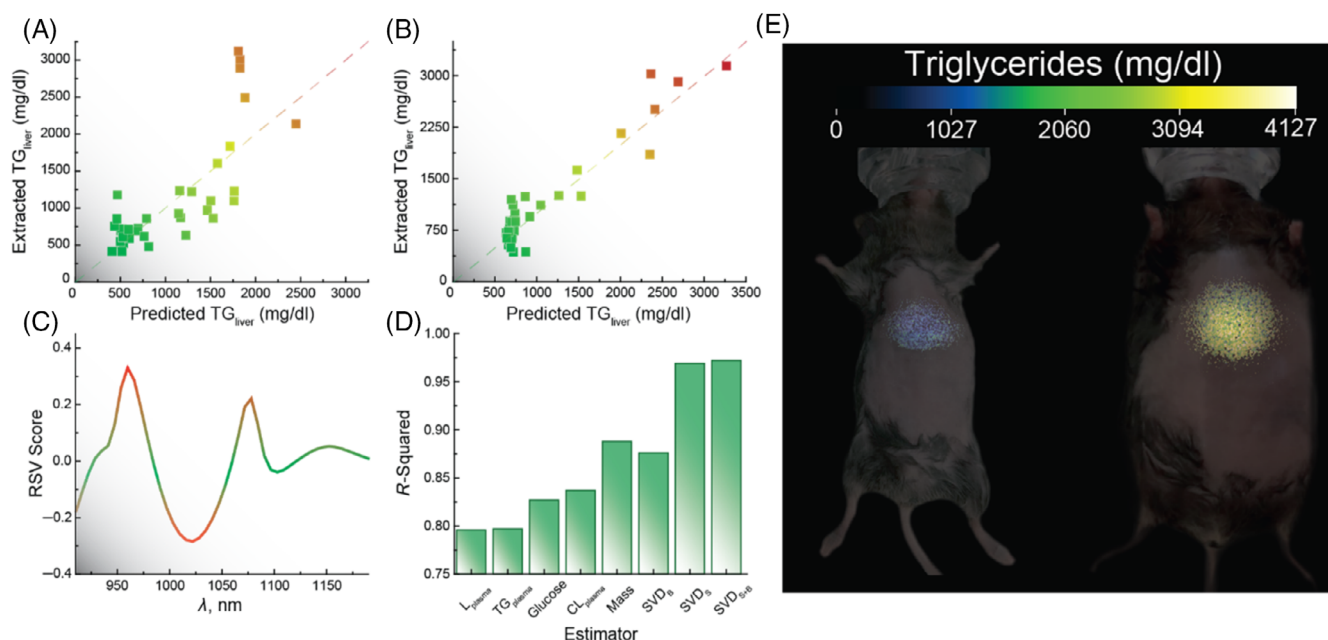


FIGURE 5 Determination of density of triglycerides in the liver, TG_{liver} , through endogenous signal. (A) Comparison between the real value of TG_{liver} and the prediction based on (A) the linear regression whose input consisted of conventional quantities (namely: Mass, glycemic levels, lipids in plasma, triglycerides in plasma, and cholesterol in plasma) easily acquired in a clinic/hospital, and (B) the linear regression of RSV_1 , that is, the spectroscopic parameters. The color change of the squares in both graphs are visual aids for identifying the transition from a healthy status to a diseased one. (C) Relative contribution of the intensities at several wavelengths to the value of RSV_1 . (D) Determination coefficient of regression models based on each of the biological parameters, the SVD of their dataset, the SVD of the endogenous spectra, and the SVD of the spectra and biological parameters. (E) Imaging of the triglycerides content in the livers of two representative mice as acquired after using the PCR regression coefficients

To explore the potential of HSI in the detection of NAFLD at different stages of development, a set of C57BL6/J male mice were separated into a control group and an affected group, which were then subdivided according to the time points in which they were sacrificed (Figure 3A). The most representative results obtained during our *in vivo* imaging protocol (see Figure 2E) are depicted in Figure 3. Taking all these data into account, one can conclude that while the reflectance signal at around 1045 nm is observed under various circumstances, the accumulation of lipids seems to be more evident when one maintains the layers of tissue found immediately above the liver. The spectra of Figure 3, therefore, suggest that the endogenous spectrum could serve as an indicator of the relative content of lipids in the liver and the surrounding layers of tissues. In a first attempt to verify how well they would account for the evolution of NAFLD, we applied SVD to the set of spectra acquired under all the conditions described in our protocol (Figure 2E). In Figure 4A–D, the first coordinates of the RSV_1 indicate that, independently of how the endogenous spectra are measured, at the very beginning of the diets, the differences between the healthy and the HFHS groups are only slightly noticed. However, as the diet progresses, the HFHS group presents deviations from the control group which, for all practical effects, keeps its value constant. The measurements performed under the four conditions all seem to point out an exponential-like change in RSV_1 .

To determine if the results of Figure 4A–D were reflective of the progress of NAFLD, the triglycerides contents in the livers of all the animals were obtained by performing a quantification colorimetric assay (sensitivity of 1 mg/dl). Representative images are included in Figure 4E. The whole set of images acquired, in turn, is included in Section S2 of Supporting Information. When analyzing the stack of acquired images, an increment in the triglycerides content is observed (Figure 4F). Its evolution is found to be like the ones shown in Figure 4A–D, suggesting, therefore, that there is a correlation of the endogenous spectra with the actual content of triglycerides in the liver of the mice. More importantly, however, it indicates that even the spectra measured under the least invasive conditions (i.e., with the shaven mice) can provide information on the progress of NAFLD. This should be expected due to the combination of endogenous signals coming from both the liver itself and the layers of tissues found on top of it. Since these layers of tissues are expected to have higher contents of fat as NAFLD progresses, the endogenous signals should change accordingly.

The possibility of using the spectra obtained with the shaven mice is particularly important because it can provide a model competitive with other techniques.

Therefore, for the sake of the discussion, all the analysis that is, hereafter, presented will be based on the endogenous spectra obtained with the shaven mice (i.e., the ones whose skin or muscle were not removed in Figure 3B). To have a standard of comparison of accuracy, we first established a method (hereafter, the “standard” method) consisting of measurements that could be easily performed in a hospital or a clinic. The input quantities were, namely mass (M), glycemic levels ($Glucose$), lipids in plasma (L_{plasma}), triglycerides in plasma (TG_{plasma}), and cholesterol in plasma (CL_{plasma}). Under those conditions, the standard method was based on the possible correlation between such quantities and the density of triglycerides in the liver. Once again SVD was applied to the dataset and a linear regression model was obtained. We will, hereafter, refer to this analysis as SVD_B , where the subindex B refers to biomedical. Figure 5A shows the comparison plot (i.e., the obtained vs the expected value of triglyceride content) of this model. It provided a coefficient of determination (R^2) of 0.87 and a root-mean-squared error (RMSE) of 470 mg/dl. Such values demonstrate that while one could qualitatively understand the dependence between parameters such as triglycerides in the blood and the density of triglycerides in the liver, the prediction that these relations offer is not so accurate and might underestimate the seriousness of NAFLD (see rightmost part of the graph).

If the endogenous spectra are taken as input, however, a linear regression based on RSV_1 provides an R^2 of 0.99 and a RMSE of 240 mg/dl (Figure 5B). We will, hereafter, refer to this analysis as SVD_S , where the subindex S refers to spectrum. These values demonstrate a higher capability of prediction when compared to what we had previously defined as the standard regression model. This is, perhaps, more easily noticed by the fact that all the points in Figure 5B get closer to the identity line ($y = x$). Thus, one could say that the density of triglycerides in the liver could be better inferred by a simple inspection of the autofluorescence spectrum than by any of the common quantities easily measured in a clinic. Another interesting aspect to notice is that even if one includes both the spectra and the clinic parameters (mass, glycemic levels, lipids in plasma, triglycerides in plasma, and cholesterol in plasma) as input for the regression model, which for sake of brevity we will refer as SVD_{S+B} , the power of prediction is not changed (Figure 5D) which indicates that most of the relevant information is already contained in the endogenous spectra.

The applications implied by Figure 5B, however, are not limited to simple detection of NAFLD. If the regression model is sufficiently reliable, it can also be extended to imaging. More specifically, lipids imaging in the liver. Having the best linear fitting determined

(Figure 5C), two mice were selected from our ensemble to image the content of lipids in their livers, which provided the in vivo gradings contained in Figure 5E. As one can see, a clear contrast is established between a healthy mouse and one that has been under a 52-week HFHS diet. When calculating the average values given by the images, their corresponding triglycerides density in the liver agrees reasonably well with the one obtained experimentally. More specifically, the lipids images of the HFHS and healthy mice provided densities of 2490 mg/dl (experimental: 2134 mg/dl) and 817 (experimental: 854 mg/dl), respectively. Such results suggest that if the HSI of endogenous signal is correlated with the spatial distribution of lipids, as obtained under ex vivo conditions with other techniques, an even more reliable image-based regression can be achieved.

4 | CONCLUSIONS

In this work, the effects of the development of fatty liver disease on the autofluorescence and reflectance of C57BL6/J male mice's abdominal region was investigated. The change in the relative contribution of the 1045 nm line was found to be highly dependent on the stage of development of NAFLD and the content of lipids in the tissues involving the liver under normal conditions. An approach based on the measurement of the endogenous spectra obtained on the surface of the skin of the mice was proposed for the prediction of the density of triglycerides in the liver. After applying SVD, a regression model with $R^2 = 0.99$ was found. This model was then applied to the narrowband hyperspectral images of the anesthetized mice to provide images corresponding to their respective contents of triglycerides in their liver. Considering the cost-effectiveness of how one could get an endogenous spectrum (infrared monochromator + 808 nm laser + Nd^{3+} sample), the method here presented could offer a noninvasive and more affordable way of detecting NAFLD at different stages of development. Additionally, since SVD is the basis of some applications involving neural networks and artificial intelligence, the results indicate that with a larger number of mice, a net could be trained for an even more accurate prediction.

CONFLICT OF INTEREST

The authors declare no conflict of interest.

DATA AVAILABILITY STATEMENT

The data that support the findings of this study are available from the corresponding author upon reasonable request.

ORCID

José Lifante  <https://orcid.org/0000-0001-8935-2448>

Daniel Jaque García  <https://orcid.org/0000-0002-3225-0667>

Erving Ximendes  <https://orcid.org/0000-0001-7182-0573>

REFERENCES

- [1] A. L. Vahrmeijer, M. Hutteman, J. R. van der Vorst, C. J. H. van de Velde, J. V. Frangioni, *Nat. Rev. Clin. Oncol.* **2013**, *10*, 507.
- [2] S. Gioux, H. S. Choi, J. V. Frangioni, *Mol. Imaging* **2010**, *9*, 237.
- [3] S. Andersson-Engels, C. Klinteberg, K. Svanberg, S. Svanberg, *Phys. Med. Biol.* **1997**, *42*, 815.
- [4] I. J. Bigio, J. R. Mourant, *Phys. Med. Biol.* **1997**, *42*, 803.
- [5] W. Rettig, H. Seifert, S. Schrader, B. Strehmel, *Applied Fluorescence in Chemistry, Biology and Medicine*, Springer, Heidelberg, 1999.
- [6] J. Zhao, D. Zhong, S. Zhou, *J. Mater. Chem. B* **2018**, *6*, 349.
- [7] A. Sharma, M. Majdinasab, R. Khan, Z. Li, A. Hayat, J. L. Marty, *Nano-Struct. Nano-Objects* **2021**, *27*, 100774.
- [8] J. Lifante, Y. Shen, E. Ximendes, E. Martín Rodríguez, D. H. Ortgies, *J. Appl. Phys.* **2020**, *128*, 171101.
- [9] W. Lohmann, E. Paul, *Naturwissenschaften* **1988**, *75*, 201.
- [10] M. Monici, *Biotechnology Annual Review*, Vol. 11, Elsevier, Amsterdam, **2005**, p. 227.
- [11] J. Lifante, B. Rosal, I. Chaves-Coira, N. Fernández, D. Jaque, E. Ximendes, *J. Biophotonics* **2020**, *13*, e202000154.
- [12] G. Bottirol, A. C. Croce, in *Comprehensive Series in Photochemical & Photobiological Sciences* (Eds: G. Palumbo, R. Pratesi), Royal Society of Chemistry, London, **2007**, p. 189. <https://doi.org/10.1039/9781847551207-00189>
- [13] A. C. Croce, G. Bottirol, *Eur. J. Histochem.* **2014**, *58*, 2461.
- [14] F. Crespi, A. C. Croce, S. Fiorani, B. Masala, C. Heidebreder, G. Bottirol, *Lasers Surg. Med.* **2004**, *34*, 39.
- [15] W. S. Kunz, W. Kunz, *Biochim. Biophys. Acta* **1985**, *841*, 237.
- [16] M. Wolman, *Pathobiol. Annu.* **1980**, *10*, 253.
- [17] D. N. Palmer, G. Barns, D. R. Husbands, R. D. Jolly, *J. Biol. Chem.* **1986**, *261*, 1773.
- [18] M. L. Katz, G. E. Eldred, W. G. Robison, *Mech. Ageing Dev.* **1987**, *39*, 81.
- [19] R. D. Fugate, P. Song, *Biochim. Biophys. Acta* **1980**, *625*, 28.
- [20] F. W. J. Teale, G. Weber, *Biochem. J.* **1957**, *65*, 476.
- [21] S. L. Marcus, R. S. Sobel, A. L. Golub, R. L. Carroll, S. Lundahl, D. G. Shulman, *J. Clin. Laser Med. Surg.* **1996**, *14*, 59.
- [22] J. R. Lakowicz, H. Szmajcinski, K. Nowaczyk, M. L. Johnson, *Proc. Natl. Acad. Sci. U. S. A.* **1992**, *89*, 1271.
- [23] R. Moll, W. W. Franke, D. L. Schiller, B. Geiger, R. Krepler, *Cell* **1982**, *31*, 11.
- [24] D. P. Thornhill, *Biochem. J.* **1975**, *147*, 215.
- [25] J. C. Kennedy, R. H. Pottier, D. C. Pross, *J. Photochem. Photobiol. B* **1990**, *6*, 143.
- [26] W.-C. Lin, S. A. Toms, E. D. Jansen, A. Mahadevan-Jansen, *IEEE J. Select. Topics Quantum Electron.* **2001**, *7*, 996.
- [27] X. Han, H. Lui, D. I. McLean, H. Zeng, *J. Biomed. Opt.* **2009**, *14*, 024017.
- [28] A. C. Croce, A. Ferrigno, G. Santin, M. Vairetti, G. Bottirol, *J. Biophoton.* **2014**, *7*, 810.
- [29] N. Chalasani, Z. Younossi, J. E. Lavine, M. Charlton, K. Cusi, M. Rinella, S. A. Harrison, E. M. Brunt, A. J. Sanyal, *Hepatol.ogy* **2018**, *67*, 328.

- [30] A. C. Croce, A. Ferrigno, G. Bottirollo, M. Vairetti, *Liver Int.* **2018**, 38, 1160.
- [31] A. C. Croce, A. Ferrigno, L. G. di Pasqua, C. Berardo, V. M. Piccolini, V. Bertone, G. Bottirollo, M. Vairetti, *J. Photochem. Photobiol. B* **2016**, 164, 13.
- [32] C. Antunes, M. Azadfar, G. J. Hoilat, M. Gupta, *StatPearls*, StatPearls Publishing, Orlando, **2021**.
- [33] J. Yu, S. Marsh, J. Hu, W. Feng, C. Wu, *Gastroenterol. Res. Pract.* **2016**, 2016, 1.
- [34] D. E. Kleiner, E. M. Brunt, M. van Natta, C. Behling, M. J. Contos, O. W. Cummings, L. D. Ferrell, Y. C. Liu, M. S. Torbenson, A. Unalp-Arida, M. Yeh, A. J. McCullough, A. J. Sanyal, Nonalcoholic Steatohepatitis Clinical Research Network, *Hepatology* **2005**, 41, 1313.
- [35] M. Papatheodoridi, E. Cholongitas, *Curr. Pharm. Des.* **2019**, 24, 4574.
- [36] S. Diao, G. Hong, A. L. Antaris, J. L. Blackburn, K. Cheng, Z. Cheng, H. Dai, *Nano Res.* **2015**, 8, 3027.
- [37] National Guideline Centre (UK), *Non-Alcoholic Fatty Liver Disease: Assessment and Management*, National Institute for Health and Care Excellence (NICE), London, **2016**.
- [38] R. Jiménez-Agüero, J. I. Emparanza, A. Beguiristain, L. Bujanda, J. M. Alustiza, E. García, E. Hijona, L. Gallego, J. Sánchez-González, M. J. Perugorria, J. I. Asensio, S. Larburu, M. Garmendia, M. Larzabal, M. P. Portillo, L. Aguirre, J. M. Banales, *BMC Med.* **2014**, 12, 137.
- [39] A. Kasahara, N. Hayashi, K. Kurosawa, Y. Sasaki, N. Sato, T. Kamada, *Hepatology* **1986**, 6, 87.
- [40] N. Hanaoka, N. Uedo, A. Shiotani, T. Inoue, Y. Takeuchi, K. Higashino, R. Ishihara, H. Iishi, K. Haruma, M. Tatsuta, *J. Gastroenterol. Hepatol.* **2010**, 25, 1844.
- [41] S. Ranjit, A. Dvornikov, E. Dobrinskikh, X. Wang, Y. Luo, M. Levi, E. Gratton, *Biomed. Opt. Express* **2017**, 8, 3143.
- [42] A. A. Gowen, Y. Feng, E. Gaston, V. Valdramidis, *Talanta* **2015**, 137, 43.
- [43] P. Mishra, A. Herrero-Langreo, P. Barreiro, J. M. Roger, B. Diezma, N. Gorretta, L. Lleó, *J. Near Infrared Spectrosc.* **2015**, 23, 15.
- [44] P. Mishra, C. B. Y. Cordella, D. N. Rutledge, P. Barreiro, J. M. Roger, B. Diezma, *J. Food Eng.* **2016**, 168, 7.
- [45] A. Yakovliev, R. Ziniuk, D. Wang, B. Xue, L. O. Vretik, O. A. Nikolaeva, M. Tan, G. Chen, Y. L. Slominskii, J. Qu, T. Y. Ohulchanskyy, *Nanoscale Res. Lett.* **2019**, 14, 243.
- [46] R. Nachabé, B. H. W. Hendriks, A. E. Desjardins, M. van der Voort, M. B. van der Mark, H. J. C. M. Sterenborg, *J. Biomed. Opt.* **2010**, 15, 037015.
- [47] P. Mishra, M. S. M. Asaari, A. Herrero-Langreo, S. Lohumi, B. Diezma, P. Scheunders, *Biosyst. Eng.* **2017**, 164, 49.
- [48] J. M. Amigo, H. Babamoradi, S. Elcoroaristizabal, *Anal. Chim. Acta* **2015**, 896, 34.
- [49] M. E. Wall, A. Rechtsteiner, L. M. Rocha, in *A Practical Approach to Microarray Data Analysis* (Eds: D. P. Berrar, W. Dubitzky, M. Granzow), Kluwer Academic Publishers, New York, **2003**, p. 91. https://doi.org/10.1007/0-306-47815-3_5
- [50] R. Kannan, S. Vempala, *FNT Theor. Comput. Sci.* **2008**, 4, 157.

SUPPORTING INFORMATION

Additional supporting information can be found online in the Supporting Information section at the end of this article.

How to cite this article: J. Lifante, M. de la Fuente-Fernández, M. Román-Carmena, N. Fernandez, D. Jaque García, M. Granado, E. Ximendes, *J. Biophotonics* **2022**, e202200208. <https://doi.org/10.1002/jbio.202200208>